Mon. Not. R. Astron. Soc. **316**, 929–942 (2000)

The mass of the Andromeda galaxy

N. W. Evans[1]★ and M. I. Wilkinson[1,2]★
[1]*Theoretical Physics, Department of Physics, 1 Keble Road, Oxford OX1 3NP*
[2]*Institute of Astronomy, Madingley Road, Cambridge CB3 0HA*

Accepted 2000 April 11. Received 2000 April 5; in original form 1999 November 25

ABSTRACT

This paper argues that the Milky Way galaxy is probably the largest member of the Local Group. The evidence comes from estimates of the total mass of the Andromeda galaxy (M31) derived from the three-dimensional positions and radial velocities of its satellite galaxies, as well as the projected positions and radial velocities of its distant globular clusters and planetary nebulae. The available data set comprises 10 satellite galaxies, 17 distant globular clusters and nine halo planetary nebulae with radial velocities. We find that the halo of Andromeda has a mass of $\sim 12.3^{+18}_{-6} \times 10^{11}\,\mathrm{M}_{\odot}$, together with a scalelength of $\sim$90 kpc and a predominantly isotropic velocity distribution. For comparison, our earlier estimate for the Milky Way halo is $19^{+36}_{-17} \times 10^{11}\,\mathrm{M}_{\odot}$. Although the error bars are admittedly large, this suggests that *the total mass of M31 is probably less than that of the Milky Way.* We verify the robustness of our results to changes in the modelling assumptions and to errors caused by the small size and incompleteness of the data set.

Our surprising claim can be checked in several ways in the near future. The numbers of satellite galaxies, planetary nebulae and globular clusters with radial velocities can be increased by ground-based spectroscopy, while the proper motions of the companion galaxies and the unresolved cores of the globular clusters can be measured using the astrometric satellites *Space Interferometry Mission* (*SIM*) and *Global Astrometric Interferometer for Astrophysics* (*GAIA*). Using 100 globular clusters at projected radii $20 \lesssim R \lesssim 50$ kpc with both radial velocities and proper motions, it will be possible to estimate the mass within 50 kpc to an accuracy of $\sim$20 per cent. Measuring the proper motions of the companion galaxies with *SIM* and *GAIA* will reduce the uncertainty in the total mass caused by the small size of the data set to $\sim$22 per cent.

Key words: celestial mechanics, stellar dynamics – galaxies: individual: M31 – galaxies: kinematics and dynamics – Local Group.

1 INTRODUCTION

The aim of this paper is to obtain an accurate estimate of the total mass of the halo of the Andromeda galaxy (M31). The best probes of the mass distribution at large distances are the satellite galaxies and the distant globular clusters. The gas rotation curve can be tracked only out to $\sim$30 kpc (e.g. Roberts & Whitehurst 1975; Hodge 1992), and so – as is the case for the Milky Way – the most substantial clues as to the large-scale mass distribution come from statistical analyses of the satellite kinematics.

The Local Group has two prominent subgroups of satellites centred on its two largest members, the Milky Way and the Andromeda galaxies (e.g. van den Bergh 1999a). A number of authors have already studied the problem of estimating the mass of the Milky Way from its satellite subgroup (e.g. Little & Tremaine 1987; Kulessa & Lynden-Bell 1992; Kochanek 1996). The most recent estimate by Wilkinson & Evans (1999, hereafter WE99) found a total mass of $\sim 1.9 \times 10^{12}\,\mathrm{M}_{\odot}$ and an extent of $\sim$170 kpc. By contrast, until recently, the companion problem of estimating the mass of the Andromeda galaxy from its satellite subgroup has received hardly any attention. Hodge (1992) lists a number of determinations of the mass of M31, but almost all use either the optical and radio rotation curves (e.g. Rubin & Ford 1970) or the inner globular clusters (e.g. Hartwick & Sargent 1974; van den Bergh 1981), and so are really measurements of the mass within $\sim$30 kpc. Recently, Courteau & van den Bergh (1999) estimated the mass of the M31 halo using only seven satellite galaxies. An analysis of all available data on objects outside $\sim$20 kpc has not been carried out to date.

It is especially timely to look at the problem of determining the mass and the extent of the Andromeda halo now. First, the last few

★ E-mail: w.evans1@physics.oxford.ac.uk (NWE); mark@ast.cam.ac.uk (MIW)

years have seen the discovery of a number of faint dwarf spheroidal companions of Andromeda (see, e.g. Armandroff & Da Costa 1999) as a result of two ongoing surveys of the sky around Andromeda. To date, one of these surveys (Armandroff & Da Costa 1999) has covered 1550 square degrees, while the second (Karachentsev & Karachentseva 1999) has scanned a circular area of radius 22 degrees centred on M31. The quantitative completeness limits of these surveys are not yet available. Armandroff & Da Costa claim that their detection of And V with absolute $M_V \sim -10.2$ is highly significant, and maintain that they have the sensitivity to detect still fainter objects, such as dwarf spheroidals with $M_V \sim -8.5$. Complementing these programmes are the ongoing radial velocity surveys of M31 globular clusters (Perrett et al. 1999) and halo planetary nebulae (Ford et al. 1989). The data set is likely to increase substantially in richness over the next few years, suggesting that more detailed models of the dynamics of the outer parts of M31 are warranted. Second, a number of groups are conducting pixel lensing experiments towards Andromeda (e.g. Crotts & Tomaney 1996; Kerins et al. 2000). The lenses may lie in the haloes of the Milky Way and M31, as well as the disc of the Milky Way and the bulge and disc of M31. Fortunately, there is a possible diagnostic of microlensing by M31's halo. As the galaxy is highly inclined, lines of sight to the far side pass through more of the M31 halo than those to the near side (Crotts 1992; Kerins et al. 2000). However, the amplitude of this near–far disc asymmetry depends on how extensive and massive the halo of Andromeda really is (Evans & Wilkinson 2000).

In Section 2 we outline the properties of our halo model, deriving both projected properties and simple distribution functions (DFs). Section 3 describes our models for the satellite galaxies, the globular clusters and the planetary nebulae, as well as the available data set. In Section 4 the mass estimator algorithm of Little & Tremaine (1987) is adapted to the case when only projected data are available. For the satellite galaxies, the three-dimensional position with respect to Andromeda's centre and the line-of-sight velocities are known. For the globular clusters and halo planetary nebulae, only the projected positions and line-of-sight velocities are available. The next two sections present our analysis of the data and estimates of the mass and extent of the Andromeda galaxy halo, together with the errors caused by incompleteness and small-number statistics. In Section 7 we summarize our conclusions and describe the prospects for the future.

2 A MODEL OF THE ANDROMEDA HALO

2.1 The density and projected mass

A simple representation of the Andromeda halo has a roughly flat rotation curve out to an unknown cut-off. The TF (or truncated, flat rotation curve) model examined in detail by WE99 has exactly these properties, as well as the virtue of analytical simplicity. The potential–density pair is

$$\rho(r) = \frac{M}{4\pi}\frac{a^2}{r^2(r^2+a^2)^{3/2}}, \qquad \psi(r) = v_0^2 \log\left(\frac{\sqrt{r^2+a^2}+a}{r}\right), \tag{1}$$

where M is the total mass of the halo, and a is a measure of the extent. The rotation curve is flat, with amplitude $v_0 = \sqrt{GM/a}$ in the inner parts. In modelling the halo of Andromeda, we assume $v_0 = 240\,\mathrm{km\,s^{-1}}$. This gives a circular velocity of $235\,\mathrm{km\,s^{-1}}$ at a radius of 30 kpc, which is in agreement with Hodge (1992, chapter 7).

As we observe M31 in projection, it is helpful to have available the projected properties of our halo model. Mateo (1998), following Karachentsev & Makarov (1996), estimates the distance D of M31 as 770 kpc, although there is still some uncertainty as to this value (cf. Feast 1999). For an observer at finite distance D, the projected surface density Σ is

$$\Sigma(R) = \left(2\int_R^D \mathrm{d}r + \int_D^\infty \mathrm{d}r\right)\frac{r}{\sqrt{r^2-R^2}}\rho(r), \tag{2}$$

from which we obtain

$$\Sigma(R) = \frac{M}{4\pi a}\left\{\frac{1}{R}\left[\arctan\left(\frac{a}{R}\frac{\sqrt{1-R^2/D^2}}{\sqrt{1+a^2/D^2}}\right)+\arctan\left(\frac{a}{R}\right)\right] - \frac{a}{(R^2+a^2)}\left(1+\frac{\sqrt{1-R^2/D^2}}{\sqrt{1+a^2/D^2}}\right)\right\}. \tag{3}$$

The usefulness of our model (1) derives from the fact that the density can be written in terms of the potential as

$$\rho(\psi) = \frac{M}{4\pi a^3}\frac{\sinh^5(\psi/v_0^2)}{\cosh^3(\psi/v_0^2)}. \tag{4}$$

This is the crucial formula for obtaining distribution functions (DFs) which are analytically tractable. This is the problem to which we now turn.

2.2 The velocity distributions

As we wish to be certain of the robustness of our results, we will analyse the data set with two different kinds of velocity distributions. A first possibility is to use the Ansatz (e.g. Hénon 1973; WE99)

$$F(\varepsilon, l) = l^{-2\beta} f(\varepsilon), \tag{5}$$

where

$$f(\varepsilon) = \frac{2^{\beta-3/2}}{\pi^{3/2}\Gamma(m-1/2+\beta)\Gamma(1-\beta)} \times \frac{\mathrm{d}}{\mathrm{d}\varepsilon}\left[\int_o^\varepsilon \mathrm{d}\psi \frac{\mathrm{d}^m r^{2\beta}\rho}{\mathrm{d}\psi^m}(\varepsilon-\psi)^{\beta-3/2+m}\right]. \tag{6}$$

Here, m is an integer whose value is chosen such that the integral in (6) converges. For such a DF, the velocity dispersions $\langle v_\phi^2\rangle$ and $\langle v_\theta^2\rangle$ are equal, and there is a constant orbital anisotropy $\beta = 1 - \langle v_\theta^2\rangle/\langle v_r^2\rangle$. The properties of these DFs are discussed fully in WE99.

A second possibility is to assume that the DFs depend on the binding energy ε and the angular momentum per unit mass l through the Ansatz (Osipkov 1979; Merritt 1985)

$$F(\varepsilon, l) = f(Q), \qquad Q = \varepsilon - \frac{l^2}{2r_a^2}, \tag{7}$$

where r_a is the anisotropy length-scale. These DFs have the property that for $r < r_a$ the velocity distribution is roughly isotropic, while for $r > r_a$ it tends towards radial anisotropy. For any

population with density ρ, the Osipkov–Merritt DF is given by

$$f(Q) = \frac{1}{2\sqrt{2}\pi^2}\int_0^Q \frac{\mathrm{d}\psi}{\sqrt{Q-\psi}}\frac{\mathrm{d}^2}{\mathrm{d}\psi^2}\left[\left(1+\frac{r^2}{r_\mathrm{a}^2}\right)\rho(r)\right]. \quad (8)$$

Inserting (4) into (8), we obtain

$$f(Q) = \frac{M}{2\sqrt{2}\pi^3 a^3 v_0^3}\int_0^{Q/v_0^2}\frac{\mathrm{d}\phi}{\sqrt{Q/v_0^2-\phi}} \times\left[\tanh\phi\sinh^2\phi+\left(1-\frac{3a^2}{2r_\mathrm{a}^2}\right)\tanh^3\phi +3\left(1-\frac{a^2}{r_\mathrm{a}^2}\right)\tanh^3\phi\,\mathrm{sech}^2\phi+\frac{3a^2}{2r_\mathrm{a}^2}\tanh\phi\right]. \quad (9)$$

The integral can be easily evaluated using Gaussian quadrature, and Fig. 1 presents examples of these DFs for several values of the anisotropy radius r_a. The DF is everywhere positive, provided that $r_\mathrm{a} \geq 0.092a$.

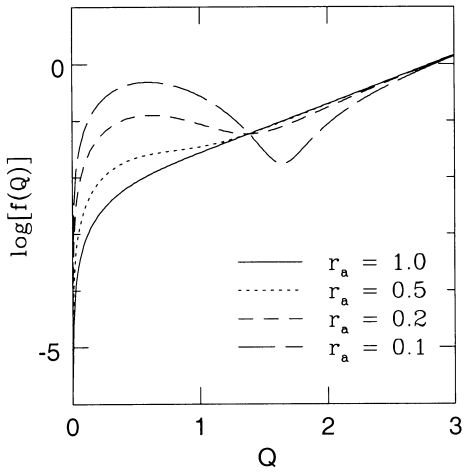

Figure 1. Osipkov–Merritt type DFs for a TF model potential. A range of values of r_a are plotted. Units with $G = M = a = 1$.

The radial velocity dispersion $\langle v_\mathrm{r}^2\rangle$ is given by

$$\langle v_\mathrm{r}^2\rangle = \frac{v_0^2(r^2+a^2)^{1/2}}{2a^5(1+r^2/r_\mathrm{a}^2)}\left[2a^2r^2+a^4\left(1-\frac{r^2}{r_\mathrm{a}^2}\right) +r^2(a^2+r^2)\left(\frac{a^2}{r_\mathrm{a}^2}-2\right)\log\left(1+\frac{a^2}{r^2}\right)\right]. \quad (10)$$

As $r \to \infty$, $\langle v_\mathrm{r}^2\rangle \to 0$, and as $r \to 0$, $\langle v_\mathrm{r}^2\rangle \to v_0^2/2$. The anisotropy parameter $\beta = 1 - \langle v_\theta^2\rangle/\langle v_\mathrm{r}^2\rangle$, which is a measure of the anisotropy of the velocity ellipsoid at radius r, is related to r_a via

$$\beta(r) = \frac{r^2}{r_\mathrm{a}^2+r^2}. \quad (11)$$

This result (11) holds true for any DFs of the Osipkov–Merritt form.

3 THE DATA

In this section we present the observational data which we use to estimate the total mass. Data are available for three halo tracer populations, namely the dwarf satellite galaxies, the outer globular clusters and the halo planetary nebulae. Each of these populations has different kinematics and so requires a different DF.

3.1 The satellites

Table 1 presents the available data on the satellite galaxies of M31 which have published radial velocity measurements. A number of recent papers have contained similar tables (Mateo 1998; Courteau & van den Bergh 1999; Lynden-Bell 1999; van den Bergh 1999b). These authors all agree that the first eight satellites in our table are definite members of the M31 subgroup of Local Group galaxies. We follow Courteau & van den Bergh (1999) in omitting both WLM (included by Lynden-Bell) and EGB0247+63 (included by both Mateo and Lynden-Bell) from our list. These exclusions are made on the basis of distance estimates – the current distance estimate for WLM (Lee, Freedman & Madore 1993) locates it more than 800 kpc from M31, while the current distance estimate of 2.2 Mpc for EGB0247+63 (Karachentsev, Tikhonov & Sazonova 1994) places it well outside the Local

Table 1. Data on the radial velocities of M31 and its dwarf satellites. Listed are Galactic coordinates (ℓ, b) and heliocentric distances (s and s_M) in kpc, as given by Courteau & van den Bergh (1999) and by Mateo (1999), respectively. Also given are the observed heliocentric radial velocities ($v_\odot$) in $\mathrm{km\,s^{-1}}$, together with actual and projected distances from the centre of M31 (r and R) in kpc (using the distances of Courteau & van den Bergh 1999), corrected heliocentric radial velocities ($v_{\mathrm{r}\odot}$) in $\mathrm{km\,s^{-1}}$ (in which the solar motion within the Milky Way and the radial motion of the Milky Way towards M31 are removed) and object type. See Section 5.1 for a discussion of the velocity corrections. For M31, the distance is taken from Karachentsev & Makarov (1996), while the radial velocity is from Courteau & van den Bergh (1999). For the satellites, all data in columns 3, 4, 5 and 7 are from Courteau & van den Bergh (1999), with the exception of the radial velocity of And II which is given by Côté et al. (1999).

Name	Alias	ℓ	b	s	s_M	$v_\odot$	r	R	$v_{\mathrm{r}\odot}$	Type
M31	NGC 224	121.2	−21.6	770	–	−301	–	–	–	SbI–II
M32	NGC 221	121.2	−22.0	760	805 ± 35	−205 ± 3	11	5	95	E2
NGC 205	M110	120.7	−21.1	760	815 ± 35	−244 ± 3	13	8	58	dSph
NGC 147	UGC 326	119.8	−14.3	660	725 ± 45	−193 ± 3	144	100	118	dSph/dE5
NGC 185	UGC 396	120.8	−14.5	660	620 ± 25	−202 ± 7	141	95	107	dSph/dE3
M33	NGC 598	133.6	−31.5	790	840 ± 50	−181 ± 3	203	198	72	ScII–III
IC 10	UGC 192	119.0	−3.3	660	825 ± 50	−344 ± 5	253	243	−29	dIrr
And II	–	128.9	−29.2	700	660 ± 100	−188 ± 3	149	138	82	dSph
LGS3	Pisces	126.8	−40.9	810	810 ± 60	−286 ± 4	276	262	−38	dIrr/dSph
Pegasus	DDO 210	94.8	−43.5	760	955 ± 50	−182 ± 2	409	399	86	dIrr/dSph
IC 1613	DDO 8	129.7	−60.6	720	700 ± 35	−232 ± 5	505	489	−58	IrrV

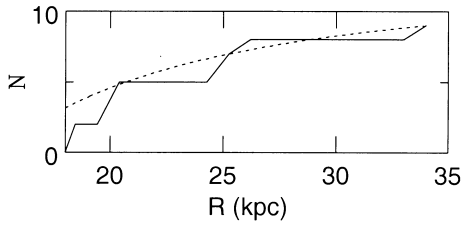

Figure 2. Cumulative number plot for the satellite galaxies. Also shown is a dotted curve representing the distribution from the assumed model, namely equation (12) with $a_s = 250\,\mathrm{kpc}$.

Group. Since Pegasus and IC 1613 both lie closer to M31 than they do to the Milky Way, we have included them in our sample, following Mateo (1998) and Lynden-Bell (1999). This is also suggested by the three-dimensional diagram of the Local Group provided by Grebel (1999). However, van den Bergh (1999a) excludes both these satellites from his list of the M31 subgroup. One other possible uncertainty in the data set is the fact that the galaxies NGC 147 and NGC 185 may form a binary system (van den Bergh 1998). The data presented recently in the literature are in good agreement with each other, except for the distance estimates for the satellites. For this reason, we have included in Table 1 the distances from Mateo (1998) and Courteau & van den Bergh (1999) to give an indication of the true uncertainties.

To model the data in Table 1, let us assume that the satellite distribution is spherically symmetric about the centre of M31, and that the density ρ_s is a TF profile with scalelength a_s:

$$\rho_s \propto \frac{a_s^2}{r^2(r^2 + a_s^2)^{3/2}}. \tag{12}$$

Fig. 2 shows how the cumulative number of satellites varies with distance from M31. The figure also shows the profile corresponding to a TF density model with $a_s = 250\,\mathrm{kpc}$ (dashed curve), which we adopt as our standard model of the satellite number density profile. We show later that our mass estimates are not overly sensitive to the choice of this scalelength. DFs for the satellites can be constructed both of constant anisotropy (6) and of Osipkov–Merritt form (8).

3.2 The globular clusters

M31 has approximately 300–400 globular clusters (Hodge 1992; Fusi Pecci et al. 1993). The system comprises a rotating disc of metal-rich clusters surrounded by a spherically symmetric, slowly rotating distribution of metal-poor clusters (Elson & Walterbos 1988). The latter are of most interest to us here, as they probe the gravity field at large distances. Table 2 presents the published data on the 17 globular clusters which lie at distances exceeding $\sim$20 kpc in projection from the centre of M31 and for which radial velocities are available.

To model the globular cluster data, let us extend the idea of isothermal populations (e.g. Binney & Tremaine 1987; Evans 1993) to the TF galaxy model. Let us consider a DF of the form

$$f(Q) = \rho_0 \left(\frac{n}{2\pi v_0^2}\right)^{3/2} \exp\left(\frac{nQ}{v_0^2}\right), \tag{13}$$

where ρ_0 is a normalization factor, and n is chosen to fit the number density profile. Crampton et al. (1985) analysed a large sample of M31 globular clusters, and argued that the radial profile

Table 2. Data on the radial velocities of the outer globular clusters of M31. Listed are Galactic coordinates (ℓ, b), observed heliocentric radial velocities $(v_\odot)$ in $\mathrm{km\,s^{-1}}$, together with projected distances R from the centre of M31 in kpc and corrected heliocentric radial velocities $(v_{r\odot})$ in $\mathrm{km\,s^{-1}}$ (in which the solar motion within the Milky Way and the radial motion of the Milky Way towards M31 are removed). See Section 5.1 for a discussion of the velocity corrections. Sources: (a) Federici et al. (1993) (b) Kent, Huchra & Stauffer (1989) (c) Perrett et al. (private communication) (d) Barmby et al. (2000). The designation S refers to the catalogue of Sargent et al. (1977).

Name	ℓ	b	$v_\odot$	R	$v_{r\odot}$
S219[d]	121.2	−23.0	−315 ± 2	19.5	−17
S352[b]	122.7	−21.2	−325 ± 20	19.5	−27
S9[d]	119.9	−20.7	−215 ± 26	19.6	89
S14[c]	119.9	−22.5	−423 ± 12	19.7	−121
S22[c]	120.2	−22.7	−374 ± 12	19.7	−73
S343[c]	122.3	−20.4	−253 ± 12	20.4	47
S13[b]	120.0	−20.5	47 ± 38	20.4	351
S268[d]	121.5	−20.1	−321 ± 26	20.6	−19
BA311[c]	122.4	−20.5	−97 ± 12	21.3	202
S327[c]	122.0	−20.1	−258.5 ± 12	22.3	42.2
S3[a]	119.4	−20.7	−87 ± 30	24.8	218
S353[a]	122.7	−20.3	−296 ± 30	26.0	3
EX8[d]	123.3	−21.3	−154 ± 40	26.7	142
S339[a]	122.2	−19.7	33 ± 30	28.3	333
S355[a]	123.0	−22.9	−60 ± 30	28.6	235
S2[d]	119.2	−23.2	−340 ± 22	33.2	−38
S1[d]	119.0	−23.2	−332 ± 3	34.1	−29

is similar to that of the Milky Way and so declines like $r^{-3.5}$ at large radii (e.g. Djorgovski & Meylan 1994; Ashman & Zepf 1998). Pursuing this analogy, we choose the parameter n, which controls the radial fall-off, to be 3.5.

As it stands, the DF (13) describes a population with no net rotation. The outer globular cluster system of M31 rotates with a velocity of $\sim$80 $\mathrm{km\,s^{-1}}$ (Huchra, Stauffer & van Speybroeck 1982). So we build a rotating DF by

$$f_{gc}(Q) = T_{gc} f_{even}(Q) + (1 - T_{gc}) f_{odd}(Q), \tag{14}$$

where T_{gc} is a parameter that controls the streaming. The even and odd parts of the DF are given by

$$f_{even}(Q) = f(Q), \tag{15}$$

and

$$f_{odd}(Q) = \begin{cases} 2f(Q), & \text{if } v_\phi \geq 0, \\ 0, & \text{otherwise.} \end{cases} \tag{16}$$

Here, v_ϕ is the azimuthal streaming velocity, where the rotation axis is taken as perpendicular to the disc of M31. The inclination of the disc of M31 is 77°.5 (Hodge 1992). Choosing $T_{gc} = 0.3$ gives the required degree of rotation ($\sim$80 $\mathrm{km\,s^{-1}}$) of the system at the radii at which we possess data ($R \sim$ 20–30 kpc).

If we assume a TF model for the halo, the expressions for the density law ρ_{gc} and velocity dispersions $\langle v_r^2 \rangle$ corresponding to the DF (13) are quite complicated (see Wilkinson 1999). However, they can be greatly simplified when $r < r_a$ and $r < a$. This is the relevant limit, as the globular cluster data are confined to the inner parts of the halo. In this case, the density profile reduces to a simple power law with index n, namely

$$\rho_{gc}(r) \sim \rho_0 \left(\frac{2a}{r}\right)^n, \tag{17}$$

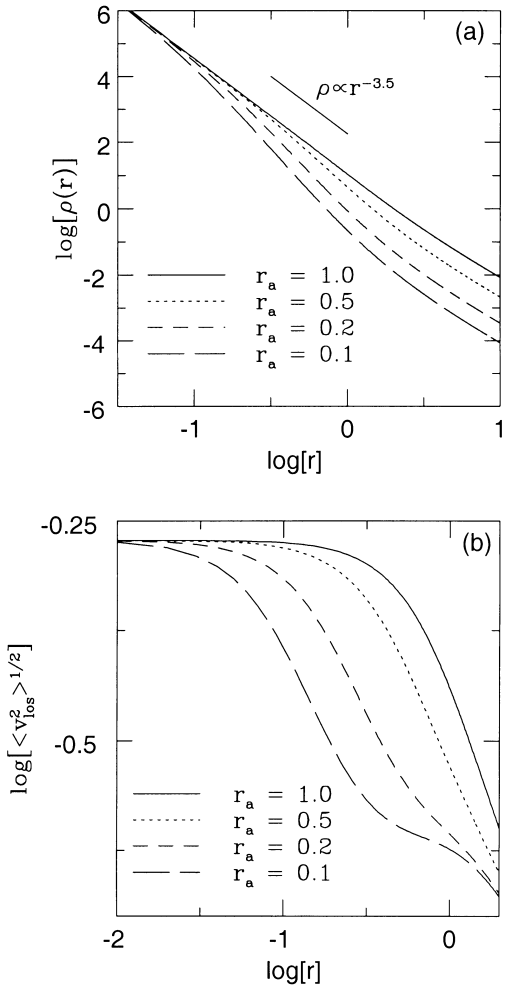

Figure 3. (a) Radial profile for the globular clusters corresponding to a density law of the form (17) with $n = 3.5$. Also shown is the slope of a simple power-law density of index 3.5. (b) Projected line-of-sight velocity dispersions for the same model profiles. Units with $G = M = a = 1$.

while the radial velocity dispersion is just

$$\langle v_r^2 \rangle \sim \frac{v_0^2}{n}. \tag{18}$$

The reason for the elegant limits is that the inner parts of the TF model look like an isothermal sphere, and so the DF (13) generates a population with a power-law density profile and a constant velocity dispersion. Fig. 3 shows the density profile and projected line-of-sight velocity dispersions for this model for a range of values of r_a, from which the isothermal limit can be distinguished.

3.3 The planetary nebulae

Planetary nebulae are luminous enough to be detected in external galaxies, and they have been increasingly exploited in recent years to estimate enclosed masses (e.g. Bridges 1999; Arnaboldi, Napolitano & Capaccioli 2000). Over 500 planetary nebulae have been detected in M31, although the total population may exceed $\sim 10^4$ (Hodge 1992). Many of these reside in the inner bulge and disc. For the outer disc and halo, the largest currently available data set is that of Nolthenius & Ford (1987), who obtained radial velocities of 34 planetary nebulae and classified them into halo and disc objects. This classification is not straightforward, as it depends on the details of the adopted warped disc model. None the less, approximately nine of the planetary nebulae are residents of the halo, and they are listed in Table 3. The planetary nebulae system rotates with a velocity of $92 \pm 43\,\mathrm{km\,s^{-1}}$ in the same sense as the rotation of the disc (Nolthenius & Ford 1987).

Table 3. Data on the radial velocities of the halo planetary nebulae of M31. Listed are Galactic coordinates (ℓ, b), observed heliocentric radial velocities ($v_\odot$) in $\mathrm{km\,s^{-1}}$, together with projected distances R from the centre of M31 in kpc and corrected heliocentric radial velocities ($v_{r\odot}$) in $\mathrm{km\,s^{-1}}$. See Section 5.1 for a discussion of the velocity corrections. Source: Nolthenius & Ford (1987).

Name	ℓ	b	$v_\odot$	R	$v_{r\odot}$
SW3/A1	120.9	−22.9	−407 ± 10	18.4	−108
SW3/A2	120.7	−22.9	−444 ± 10	18.4	−144
NE6/8	121.8	−20.2	−79 ± 10	19.7	222
SW4/6	119.8	−22.3	−263 ± 10	19.8	40
SW4/5	119.7	−22.3	−511 ± 10	20.0	−208
SW3/1	120.8	−23.4	−263 ± 10	24.4	36
SW4/2	119.3	−22.3	−349 ± 10	24.9	−46
NE6/6	122.0	−19.9	−452 ± 10	25.4	−151
NE1-2/2	123.0	−19.8	−117 ± 10	33.3	182

We model the system in a similar way to the globular clusters. We assume a DF of the form

$$f_{pn}(Q) = T_{pn} f_{even}(Q) + (1 - T_{pn}) f_{odd}(Q), \tag{19}$$

implying a density law (17). In order to fit the number density of the planetary nebulae, we choose $n = 4.8$ in the density law, as suggested by Nolthenius & Ford's (1987) fit. We pick $T_{pn} = 0.065$ to ensure that streaming velocity $\langle v_\phi \rangle \sim 92\,\mathrm{km\,s^{-1}}$. Let us note that the value of T is quite different from that obtained for the globular clusters, although the rotation velocities are comparable. The reason for this is that T depends on the choice of asymptotic fall-off n in the density law.

4 THE ALGORITHM

We derive our probability formulae using only the assumption that the halo potential of Andromeda is spherically symmetric. We seek to maximize the likelihood of a parameterised model with respect to the data $P(\mathrm{model}|\mathrm{data})$. This is given by Bayes' theorem as (see Little & Tremaine 1987 and WE99):

$$P(\mathrm{model}|\mathrm{data})P(\mathrm{data}) = P(\mathrm{model})P(\mathrm{data}|\mathrm{model}). \tag{20}$$

Here, $P(\mathrm{model})$ describes our prior beliefs as to the likelihood of the model parameters, while $P(\mathrm{data}|\mathrm{model})$ is the probability of the data given the model. For each of the S satellites of M31, the data consist of their three-dimensional positions r_i $(i = 1 \ldots S)$ with respect to the centre of Andromeda, together with their heliocentric line-of-sight velocities $v_{\odot,i}$. For the globular clusters and planetary nebulae, the three-dimensional positions are unknown. So, for each of the G globular clusters and N planetary nebulae, the data are the two-dimensional projected positions R_i $(i = 1 \ldots G + N)$ with respect to the centre of Andromeda, together with their line-of-sight velocities $v_{\odot,i}$.

4.1 Probabilities for the satellites

Let $v_{\mathrm{r}\odot,i}$ be the line-of-sight velocity corrected for the solar motion and the radial motion of M31. Then, the probability of finding a satellite at position r_i moving with line-of-sight velocity $v_{\mathrm{r}\odot,i}$ is simply

$$P(r_i, v_{\mathrm{r}\odot,i}|\mathrm{model}) = \frac{1}{\rho_{\mathrm{s}}} \int \mathrm{d}^3 v f(\varepsilon, l) \delta(v_{\mathrm{r}\odot} - v_{\mathrm{r}\odot,i}), \tag{21}$$

where ρ_{s} is the density distribution of the satellites, and $f(\varepsilon,l)$ is the DF. As some of the satellites of Andromeda lie at large angular separations from its centre, it is important to carry out the integration over the velocities perpendicular to the line of sight from the perspective of an observer at a finite distance $D = 770\,\mathrm{kpc}$ and not at infinity. Let the components of the satellite's velocity with respect to a spherical polar coordinate system oriented at Andromeda's centre be $(v_{\mathrm{r}}, v_\theta, v_\phi)$. Along any line of sight, let (v_{t}, η) be polar coordinates in the plane of projection, and $v_{\mathrm{r}\odot}$ the component along the line of sight and perpendicular to the plane of projection. Fig. 4 shows a satellite galaxy at a spherical polar distance r_i and a projected distance R_i. The line of sight subtends an angle α_i from the axis joining the observer to the centre of Andromeda, while the radius vector subtends an angle θ_i. It is straightforward to see that

$$\sin(\alpha_i + \theta_i) = R_i/r_i, \qquad \sin\alpha_i = R_i/D. \tag{22}$$

The angles α_i and θ_i are fixed for the ith satellite galaxy, since we know its distance along the line of sight. The relations between the observed velocity and the velocity components in spherical coordinates centred on M31 are

$$\begin{aligned} v_{\mathrm{r}} &= v_{\mathrm{t}} \cos\eta \sin(\theta_i + \alpha_i) - v_{\mathrm{r}\odot,i} \cos(\theta_i + \alpha_i), \\ v_\theta^2 + v_\phi^2 &= [v_{\mathrm{r}\odot,i} \sin(\theta_i + \alpha_i) + v_{\mathrm{t}} \cos\eta \cos(\theta_i + \alpha_i)]^2 \\ &\quad + v_{\mathrm{t}}^2 \sin\eta^2. \end{aligned} \tag{23}$$

Thus the required probability is given by

$$P(r_i, v_{\mathrm{r}\odot,i}|\mathrm{model}) = \frac{1}{\rho_{\mathrm{s}}(r_i)} \int_0^{\sqrt{2\psi(r_i) - v_{\mathrm{r}\odot,i}^2}} \mathrm{d}v_{\mathrm{t}} \;\; v_{\mathrm{t}} \times \int_0^{2\pi} \mathrm{d}\eta f(\varepsilon, l). \tag{24}$$

Note that the transformations (23) are used to rewrite the binding energy ε and angular momentum per unit mass l in terms of the integration variables. This formula is valid for any spherically symmetric density distribution of satellite galaxies ρ_{s}. If the observer is infinitely far away from the galaxy, then all the above formulae hold good with $\alpha_i = 0$.

4.2 Probabilities for the globular clusters and planetary nebulae

The probability of finding a globular cluster at projected radius R_i moving with line-of-sight velocity $v_{\mathrm{r}\odot,i}$ is more cumbersome, as we must integrate along the line of sight. As a result, the angle θ is no longer fixed for each object, but is a function of the distance along the line of sight z. The probability of drawing the data pair $(R_i, v_{\mathrm{r}\odot,i})$ from the projected distributions is

$$P(R_i, v_{\mathrm{r}\odot,i}|\mathrm{model}) = \frac{1}{\Sigma(R_i)} \int_{-\infty}^{\infty} \mathrm{d}z \int \mathrm{d}^3 v f(\varepsilon, l) \delta(v_{\mathrm{r}\odot} - v_{\mathrm{r}\odot,i}). \tag{25}$$

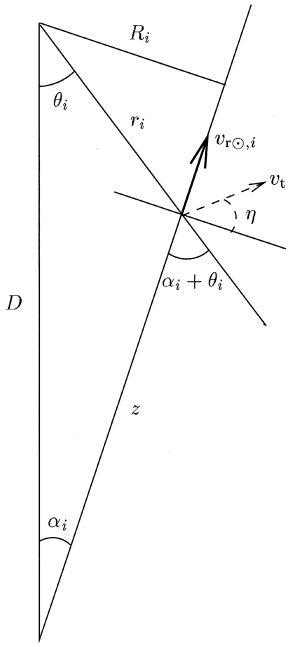

Figure 4. This figure shows a satellite at true position r_i and projected position R_i with respect to the centre of the spherical halo of the Andromeda galaxy. The angles θ_i and α_i are defined. The index i labels the number of satellites.

For an observer at finite distance D, we then obtain

$$P(R_i, v_{\mathrm{r}\odot,i}|\mathrm{model}) = \frac{R_i}{\Sigma(R_i)} \int_{\theta_{\min}}^{\theta_{\max}} \mathrm{d}\theta \,\mathrm{cosec}^2(\alpha_i + \theta) \times \int_0^{\sqrt{2\psi(\theta) - v_{\mathrm{r}\odot,i}^2}} \mathrm{d}v_{\mathrm{t}} v_{\mathrm{t}} \int_0^{2\pi} \mathrm{d}\eta f(\varepsilon, l), \tag{26}$$

where

$$\theta_{\min} = \begin{cases} a\cos(R_i/D) - a\cos(R_i/r_{\max}), & \text{if } r_{\max} < D, \\ 0, & \text{if } r_{\max} > D, \end{cases} \tag{27}$$

and

$$\theta_{\max} = a\cos(R_i/D) + a\cos(R_i/r_{\max}). \tag{28}$$

In all the above formulae, $r_{\max}$ is the solution of the equation $\psi(r_{\max}) = \frac{1}{2} v_{\mathrm{r}\odot,i}^2$, namely

$$r_{\max} = a\,\mathrm{csch}\left(\frac{v_{\mathrm{r}\odot,i}^2}{2v_0^2}\right).$$

Physically, $r_{\max}$ is the greatest radius at which the globular cluster or planetary nebula could have the line-of-sight velocity $v_{\mathrm{r}\odot,i}$ and still remain bound to the Andromeda galaxy.

We note that for an observer who is infinitely far away, all the above formulae hold good with

$$\theta_{\min} = \pi/2 - \arccos(R_i/r_{\max}), \tag{29}$$

and

$$\theta_{\max} = \pi/2 + \arccos(R_i/r_{\max}). \tag{30}$$

It is often possible to carry out the velocity integration in (26) analytically leaving only a double integral to be performed numerically.

4.3 Prior probabilities and error convolution

In any Bayesian analysis, it is necessary to specify the prior probabilities of the model parameters. We have meagre information about the anisotropy of the velocity distribution. When using constant anisotropy DFs (5), we choose $P(\beta) \propto 1/(3-2\beta)^2$, as this ensures that the ratio of radial kinetic energy to total kinetic energy is uniform. When using DFs of Osipkov–Merritt form (8), we choose a prior of $1/r_a$ for the anisotropy radius. This is the recommended choice of an unbiased prior for a parameter which can vary in the range $(0,\infty)$ (see, e.g. Kendall & Stuart 1977). In our earlier analysis of the mass of the Milky Way (WE99), we experimented with a prior on M of $1/M^2$ and found that it yielded good results. This has some advantages over $1/M$, as it reduces the probability of unrealistically large haloes. Since it is important to verify that our results are not overly sensitive to the choice of priors, Section 5 also presents results using a number of alternatives.

The projected positions of the globular clusters and planetary nebulae are known to good accuracy, as are the radial velocities of all the objects in our tracer populations. However, the distances to the satellite galaxies are uncertain. We take this into account with an error convolution function to obtain the probabilities of the observations from our theoretical probabilities. As there is no reason to assume that the observational errors are Gaussian, we use hat-box functions. These have the form

$$B(d;d_{\min},d_{\max}) = \begin{cases} \dfrac{1}{d_{\max}-d_{\min}}, & d_{\min} < d < d_{\max}, \\ 0, & \text{otherwise.} \end{cases} \tag{31}$$

Our error convolution aims to take account of two factors. First, there is the quoted error estimate associated with each distance given in Table 1. Second, there is a small, but distinct, probability ϵ that some of the published distance estimates are seriously in error due to systematic uncertainties. Therefore we choose our convolution function E to have the form (cf. Schmoldt & Saha 1998)

$$E(z;i) = (1-\epsilon)B(z;s_i-\Delta s_i, s_i+\Delta s_i) + \epsilon B(z;s_{\min},s_{\max}), \tag{32}$$

where s_i is the published distance estimate of the ith satellite with error Δs_i, and $s_{\min}$ and $s_{\max}$ are the minimum and maximum of all the published distance estimates listed in Table 1. In what follows, we assume that the probability of a rogue distance ϵ is 0.1. Section 5 presents results both for the case in which Δs_i is taken to be the quoted error on the distance measurement given in Table 1, and for the worst case in which the distance errors are assumed to be 25 per cent. This value is chosen based on the magnitudes of recent revisions of the distance estimates (see columns 5 and 6 of Table 1).

5 MASS ESTIMATES

In this section we apply the algorithm to the observational data. Section 5.1 considers only the satellite galaxies. Then, in Section 5.2, each of our three tracer populations is analysed separately before they are combined to form a single sample. The robustness of our estimates is examined in Section 5.3.

5.1 Satellite galaxies only

First, we must convert the observed heliocentric line-of-sight velocities $v_\odot$ into velocities in the rest frame of Andromeda $v_{r\odot}$. This entails removing the contributions from both the solar motion within the Galaxy and the Galactic motion towards M31. To do this, we assume a circular speed of $220\,\mathrm{km\,s^{-1}}$ at the Galactocentric radius of the Sun ($R_\odot = 8.0\,\mathrm{kpc}$) and a solar peculiar velocity of $(U,V,W) = (-9,12,7)$, where U is directed outward from the Galactic Centre, V is positive in the direction of Galactic rotation at the position of the Sun, and W is positive towards the North Galactic Pole. The line-of-sight velocity of M31, corrected for the motion of the Sun, is $v_{r,M31} = -123\,\mathrm{km\,s^{-1}}$, based on the uncorrected value of $v_{\odot,M31} = -301\,\mathrm{km\,s^{-1}}$ (Courteau & van den Bergh 1999). Some of the satellites are located at large angular distances from the centre of M31. This means that the unknown tangential velocity of M31 contaminates the observed heliocentric radial velocity. In the absence of any measurement, we assume that this unknown tangential velocity is zero. This is very reasonable, as there are no other large galaxies in the Local Group to generate angular momentum through tidal torques, and so – as Kahn & Woltjer (1959) originally argued – we are probably falling directly towards Andromeda. In order to correct for the motion towards M31, we therefore subtract the component of $v_{r,M31}$ along the line of sight to each satellite. As pointed out by Bahcall & Tremaine (1981), the large angular separations from M31 of both IC 1613 and Pegasus mean that the determination of their velocities relative to M31 depends sensitively on any tangential velocity component of M31.

As a first calculation, we analyse the satellite data set using the constant anisotropy family of DFs of the form (6). Due to the singularity in the DF that can occur at the radial orbits ($l=0$), some care is needed when carrying out the integration in (24) over the transverse velocities – the relevant substitutions are given in Appendix A. Fig. 5 presents likelihood contours in the M–β plane for the satellite data set only. The best estimate for the total mass is $8.1\times10^{11}\,\mathrm{M_\odot}$. The most likely value of β is -0.9, indicating a somewhat tangential velocity distribution. We note that the likelihood contours are elongated in the direction of the β-axis, indicating that the anisotropy is more poorly constrained than the mass. For comparison, our earlier estimate for the Milky Way halo (WE99) was $19\times10^{11}\,\mathrm{M_\odot}$. We reach the surprising conclusion that *the total mass of M31 may be less than that of the Milky Way.*

There is a second piece of evidence worth bringing forward. For an isotropic tracer population falling off like r^{-3} in a galaxy with a flat rotation curve of amplitude v_0, there is the simple result (e.g. Evans, Häfner & de Zeeuw 1997)

$$v_0^2 = 3\langle v_r^2\rangle. \tag{33}$$

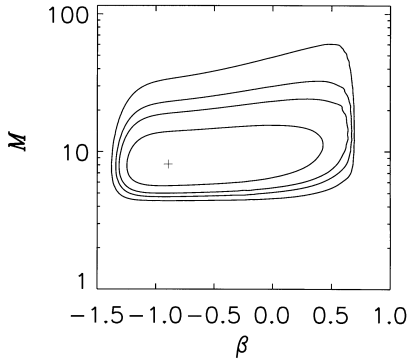

Figure 5. Likelihood contours for the total mass M (in units of $10^{11}\,\mathrm{M_\odot}$) and the anisotropy parameter β, assuming a DF of the form (6). Contours are at heights of 0.32, 0.1, 0.045 and 0.01 of peak height. Data on the satellite galaxies only have been used.

Here, $\langle v_r^2 \rangle$ is the mean square radial velocity of the sample (in the rest frame of the galaxy). Applying this formula to the data set of the Milky Way satellites gives $v_0 \sim 220\,\mathrm{km\,s^{-1}}$. This is in excellent agreement with estimates of the local circular speed, from which we conclude that the Milky Way's halo is roughly isothermal out to the distances probed by the satellites. The data set on the Andromeda satellites gives $v_0 \sim 140\,\mathrm{km\,s^{-1}}$, which is substantially less than amplitude of the HI rotation curve ($\sim 240\,\mathrm{km\,s^{-1}}$). This suggests that the isothermal region of the Andromeda halo is less than the volume sampled by the satellite galaxies.

5.2 All data

We now proceed to subject our hypothesis to serious scrutiny by modelling the data not just on the satellite galaxies, but also on the planetary nebulae and the globular clusters. For all the samples, we adopt the alternative family of DFs, namely those of Osipkov–Merritt form (8), as a precautionary check for robustness.

Fig. 6(a) shows likelihood contours in the plane of the total mass M and the anisotropy radius r_a for the planetary nebulae. This data set implies a low halo mass of $\sim 3.7 \times 10^{11}\,\mathrm{M_\odot}$ and an anisotropy radius of $\sim 66\,\mathrm{kpc}$. Given that the planetary nebulae are all located at projected radii between 18 and 34 kpc, this mass estimate must be taken as a constraint only on the mass inside a three-dimensional radius of $\sim 31\,\mathrm{kpc}$. This figure is obtained by taking the median projected radius and converting to a three-dimensional radius by multiplying by a deprojection factor of $\pi/2$. It is worth noting that the available data on the planetary nebulae are not uniformly distributed over the halo of M31, but are concentrated in two regions near the optical disc. A total mass of $3.7 \times 10^{11}\,\mathrm{M_\odot}$ implies that the mass within $\sim 31\,\mathrm{kpc}$ is $2.8 \times 10^{11}\,\mathrm{M_\odot}$.

Fig. 6(b) shows the likelihood contours obtained from the globular cluster data set. In this case, the mass estimate is $\sim 9.2 \times 10^{11}\,\mathrm{M_\odot}$, with an anisotropy radius of $\sim 86\,\mathrm{kpc}$. The globular cluster data probe a range of projected radii between 19 and 34 kpc. They are more uniformly distributed than the planetary nebulae, making this estimate more robust. A total halo mass of $9.2 \times 10^{11}\,\mathrm{M_\odot}$ implies a mass inside 40 kpc of $4.7 \times 10^{11}\,\mathrm{M_\odot}$. We note that the globular clusters are effectively probing a volume which is approximately double that probed by the planetary nebulae. The globular cluster data imply a mass inside 31 kpc of $3.8 \times 10^{11}\,\mathrm{M_\odot}$, which is somewhat larger than that implied by the planetary nebulae.

Fig. 6(c) presents the results obtained using the data on the satellite galaxies. In this case, the best mass estimate is $\sim 10.8 \times 10^{11}\,\mathrm{M_\odot}$, with an anisotropy radius of $\sim 610\,\mathrm{kpc}$. The large value of the anisotropy radius suggests that the velocity distribution is isotropic over the entire region probed by the satellites. Given that the satellites probe radii from ~ 10 to $\sim 500\,\mathrm{kpc}$, this is an estimate of the total mass of the M31 halo. In Fig. 6(d), all the data from our three populations are combined into a single data set. The mass estimate is $\sim 12.3 \times 10^{11}\,\mathrm{M_\odot}$, with an anisotropy radius of $\sim 551\,\mathrm{kpc}$. This corresponds to a halo scalelength $a \sim 91\,\mathrm{kpc}$. The value of the total mass implies masses interior to 31 and 40 kpc of $\sim 4.0 \times 10^{11}$ and $\sim 4.9 \times 10^{11}\,\mathrm{M_\odot}$,

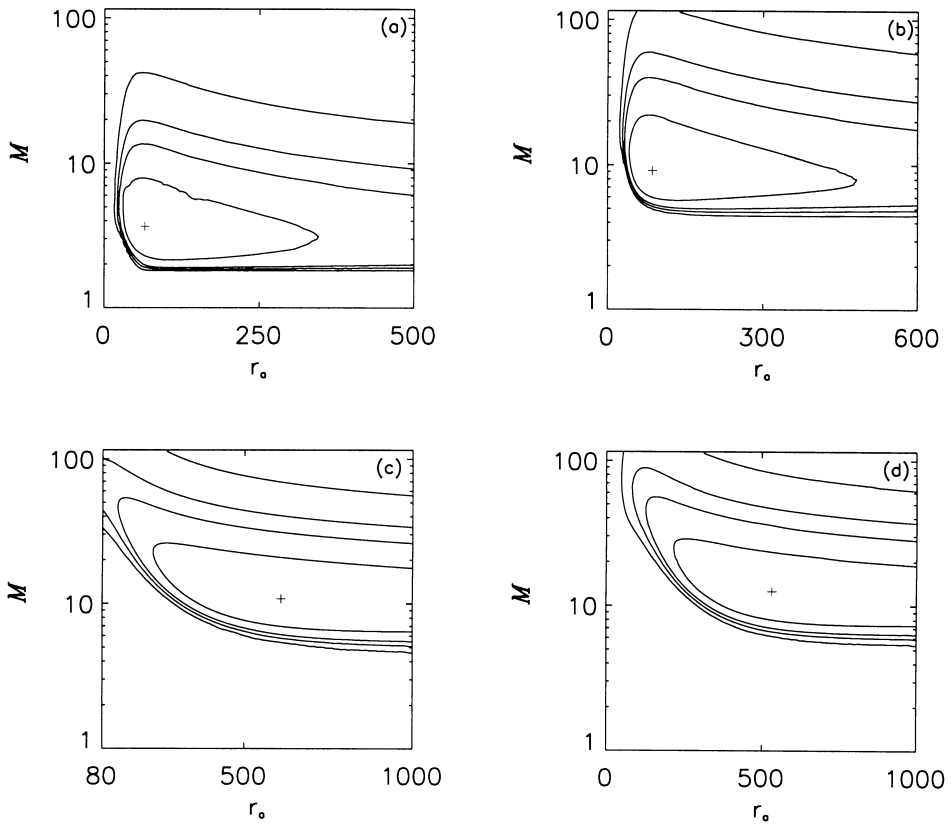

Figure 6. Likelihood contours for the total mass M (in units of $10^{11}\,\mathrm{M_\odot}$) and the anisotropy radius r_a (in kpc). Contours are at heights of 0.32, 0.1, 0.045 and 0.01 of peak height. Data used: (a) planetary nebulae only, (b) globular clusters only, (c) satellite galaxies only, (d) all data combined.

Table 4. Most likely values of M (in units of $10^{11}\,M_\odot$) and r_a (in kpc) obtained from the contour plots of Fig. 6. The corresponding values of a (in kpc) and the mass inside 30 kpc are given. The effects of changing the prior on r_a and M are illustrated.

Data	M prior	r_a prior	Most likely r_a	Most likely M	Most likely a	M (<30)
PN	$1/M^2$	$1/r_a$	66	3.7	26	2.8
PN	$1/M$	$1/r_a$	35	5.6	41	3.3
PN	$1/M^2$	1	500	3.1	21	2.5
GC	$1/M^2$	$1/r_a$	86	9.2	68	3.7
GC	$1/M$	$1/r_a$	75	11.4	85	3.8
GC	$1/M^2$	1	599	7.9	58	3.6
Sat	$1/M^2$	$1/r_a$	610	10.8	80	3.8
Sat	$1/M$	$1/r_a$	482	13.7	102	3.9
Sat	$1/M^2$	1	1000	9.7	72	3.7
All	$1/M^2$	$1/r_a$	551	12.3	91	3.8
All	$1/M$	$1/r_a$	439	15.5	115	3.9
All	$1/M^2$	1	1000	10.6	79	3.8
All	$1/M$	1	1000	12.6	95	3.9

Table 5. Table illustrating the effects of changing some of the assumed model parameters. The parameter which has been changed is given in the third column. The prior on M is $1/M^2$, and the prior on r_a is $1/r_a$. Most likely values of M (in units of $10^{11}\,M_\odot$) and r_a (in kpc) are given, together with the corresponding values of a (in kpc) and the mass inside 30 kpc. Sources for data: 1. Courteau & van den Bergh (1999) 2. Mateo (1998).

Data	Source	Comment	Most likely r_a	Most likely M	Most likely a	M (<30)
Sat	1	DF $\sim l^{-2\beta} f(\varepsilon)$	$\beta = -0.9$	8.1	60	3.6
Sat	1	Pegasus and IC 1613 omitted	128	7.2	53	3.6
All	1	Pegasus and IC 1613 omitted	114	9.4	69	3.7
All	2	Sat. distances altered	607	13.2	98	3.9
All	1	$D = 900$ kpc	615	15.7	117	3.9
All	1	$\Delta s = 25\%$	535	12.6	94	3.8
All	1	$a_s = 150$ kpc	551	13.0	97	3.9
All	1	$n_{gc} = 5$	619	10.8	80	3.8
All	1	$T_{gc} = 1$	537	12.6	94	3.8
All	1	$v_c = 270\,\mathrm{km\,s^{-1}}$	613	11.2	65	4.7
		$v_c = 200\,\mathrm{km\,s^{-1}}$	539	12.6	135	2.7

respectively. These values are in good agreement with the results obtained from the globular cluster data. The mass inside 31 kpc is greater than that implied by the planetary nebulae data – the non-uniform distribution of the planetary nebulae is the most likely cause of this discrepancy. Our final calculation assumes that all three populations have the same anisotropy radius; this seems reasonable, as the individual calculations in Figs 6(a)–(c) all yield values of r_a greater than the outermost data points, implying that the respective velocity distributions are all largely isotropic.

Table 4 summarizes the results described above and illustrates the effects of varying the prior probabilities. For the planetary nebulae data, changing the priors has some effect on the mass estimates obtained. Changing the prior on M to $1/M$ allows larger values of M, and the mass estimate rises by $\sim$50 per cent. A uniform prior on r_a naturally allows larger values of r_a, but changes the mass by only $\sim$16 per cent. For the globular cluster data, the situation is somewhat better, with the largest change being a 24 per cent increase in the mass estimate when the prior on M is changed to $1/M$. For the complete data set, allowing larger haloes produces an increase in the mass estimate of $\sim$26 per cent, which is a reasonably small change. Indeed, if we simultaneously relax both the M and r_a priors, the mass estimate changes by only $\sim$2 per cent. Given the other uncertainties in the problem (see Section 6), sensitivity to the priors is not a serious worry.

We remark that all the results in Table 4 support the hypothesis that the mass of the Andromeda halo is probably less than that of the Milky Way halo (see table 5 of WE99 as a comparison).

5.3 Robustness

We now look at the effects of altering some of the assumptions made in the modelling. The calculations are summarized in Table 5.

First, it is important to assess whether the mass estimate is strongly sensitive to any one of the data points, in a manner analogous to the effect of Leo I on mass estimates of the Milky Way. We remove each of the satellites in turn and apply the algorithm to the reduced data set. The only satellite which significantly alters the answer is Pegasus – removing Pegasus from the data set reduces the mass estimate based only on the satellites by $\sim$23 per cent. Removing any of the other satellites affects the mass estimate by less than 10 per cent. The data set used by Courteau & van den Bergh (1999) excludes both Pegasus and IC 1613. With this subsample, we obtain a low mass estimate

Table 6. Other mass estimates for M31 (out to a radius $r_{\rm max}$). All estimates have been corrected to put M31 at a distance of 770 kpc by applying the simple correction $\Delta M/M \sim \Delta D/D$, where ΔM and ΔD are the changes in the mass estimate M and the distance D to M31, respectively.

Author	Data	Mass ($10^{11}\,{\rm M}_\odot$)	$r_{\rm max}$ (kpc)
Rubin & Ford (1970)	Hα rotation curve	2.0	27
Einasto & Rümmel (1970)	Optical and radio data	2.2	25
Gottesman & Davies (1970)	21-cm rotation curve	2.5	34
Hartwick & Sargent (1974)	Globular clusters	3.8	19
Deharveng & Pellet (1975)	Hα rotation curve	1.8	22
Roberts & Whitehurst (1975)	21-cm rotation curve	4.1	33
Gunn (1975)	Local Group timing	22	–
Hodge (1975)	Tidal cut-off of companions	67	Total
Rood (1979)	Virial mass of M31 subgroup	2.9	To IC 1613
van den Bergh (1981)	Satellites	8.7	To LGS3 (∼260)
	Globular clusters	2.8	22
Braun (1991)	21-cm rotation curve	2.2	31
Courteau & van den Bergh (1999)	Satellites	13.5	To LGS3 (∼260)
This paper	Planetary nebulae	2.8	∼31
	Globular clusters	4.7	∼40
	All satellites	12.3	Total

of $7.2 \times 10^{11}\,{\rm M}_\odot$ (using our standard $1/M^2$ and $1/r_{\rm a}$ priors). For comparison, Courteau & van den Bergh obtained $13.3 \pm 1.8 \times 10^{11}\,{\rm M}_\odot$ based on the projected mass estimator of Heisler, Tremaine & Bahcall (1985).

Up to this point, we have used the distances to the satellites in Courteau & van den Bergh (1999). If, instead, we take the distances from Mateo (1998), we find that our mass estimate based on the entire data set increases by ∼7 per cent to $13.2 \times 10^{11}\,{\rm M}_\odot$. Mateo's distances imply larger separations from M31 for seven of the satellites – for example, the distance of And II from M31 is increased by 81 per cent to 270 kpc. Positioning more of the satellites at larger radii requires a larger, more massive halo to bind them. Recently, Feast (1999) has claimed that even the distance to M31 may be in serious error. He suggested that the distance modulus for M31 is 24.75 based upon a critical comparison of several distance estimates obtained using a variety of standard candles. This distance modulus implies a distance to M31 of ∼900 kpc. If this is the case, our mass estimate using the standard priors rises by 28 per cent to $15.7 \times 10^{11}\,{\rm M}_\odot$. This is caused by the increased separation of the satellites from M31 enforced by the greater distance. It is the most substantial of all the changes recorded in Table 5. Given the size of recent revisions of the distances to the satellites, it seems likely that the error bars quoted in Table 1 are rather optimistic. We therefore re-analyse the data assuming error bars of 25 per cent on all satellite distances in our error convolution. This has a negligible effect on the mass estimate.

Next, we examine the effect of changing our assumed models for the globular cluster and satellite number density laws. As discussed in Section 3.1, choosing $a_{\rm s} = 250$ kpc provides a good fit to the present satellite data set, and leaves some room for more satellites to be hiding within 250 kpc of M31. Since we do not really know how incomplete the satellite data set is, our choice of $a_{\rm s}$ may be incorrect. We therefore re-analyse the data set with $a_{\rm s} = 150$ kpc. Table 5 shows that the mass estimate changes by only 6 per cent. Similarly, choosing a larger value of n for the globular cluster number density law gives a better fit to the data at large radii, while overestimating the numbers at small radii. If we choose $n = 5$, we find that the mass estimate changes by ∼12 per cent. It is thus clear that our choice of parameters for the number densities of the tracer populations has little effect on the estimate obtained. There is also some uncertainty as to the rotation velocity of the outer globular cluster system (Elson & Walterbos 1988; Huchra, Kent & Brodie 1991), but we have verified that our results are robust to changes in this parameter.

We must also consider the possibility that our assumption regarding the normalization of the halo potential is incorrect. Up to now, we have assumed that the halo normalization $v_{\rm c} \sim 240\,{\rm km\,s^{-1}}$. If we instead take $v_{\rm c} \sim 270\,{\rm km\,s^{-1}}$, the mass estimate is reduced by ∼9 per cent, while if we reduce $v_{\rm c}$ to $200\,{\rm km\,s^{-1}}$, the mass is slightly increased by ∼2 per cent. The small size of the changes confirms that this is not a real source of uncertainty.

Table 6 summarizes previous studies of the mass of M31 to allow comparison with our results (cf. Hodge 1992, chapter 8). All the mass estimates have been corrected to a standard value of distance to M31 of 770 kpc. As in the case of the Milky Way (see fig. 13 of WE99), the inferred mass of M31 has tended to increase during the past 30 years. Our estimate actually agrees well, both with the most recent estimate of the total mass (Courteau & van den Bergh 1999) and estimates of the mass of the inner 20–30 kpc (e.g. van den Bergh 1981). The former agreement is partly fortuitous, as van den Bergh omits some satellite galaxies we have included. It is interesting to compare the results obtained using our algorithm with those which would be obtained using, for example, the projected mass estimator of Bahcall & Tremaine (1981). Using this estimator with the recommended multiplicative factor for an isotropic velocity distribution yields a mass estimate of $11.5 \times 10^{11}\,{\rm M}_\odot$, which agrees well with our results. If we instead use the factor which is recommended for use in the absence of information on the velocity distributions, we obtain the somewhat larger mass of $17.2 \times 10^{11}\,{\rm M}_\odot$.

6 ERROR ANALYSIS

This section examines the main sources of error in our estimate. The dominant problems are caused by the small size and possible incompleteness of the data set. The errors in the radial velocities are mostly insignificant, the distances to the satellite galaxies being the only quantities in the problem with large uncertainties.

6.1 The size of the data set

In order to investigate this problem, we generate 1000 synthetic

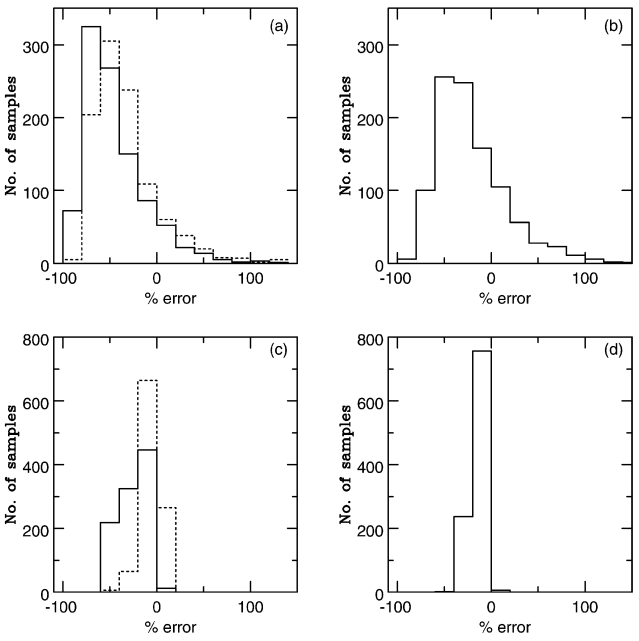

Figure 7. (a) Histogram showing the spread in mass estimates based on satellite data sets containing 10 objects (solid line) and 20 objects (broken line) at radii $20 < r < 500$ kpc from M31. Each histogram shows the number of data sets out of 1000 which yielded a given percentage error in the total mass M. (b) Histogram illustrating the effects of incompleteness in the satellite sample. Data sets of 20 satellites with different values of a_s used in the generation of the data and the analysis. See text for discussion. (c) Histogram showing the spread in mass estimates based on globular cluster data sets containing 30 objects (solid line) and 100 objects (dotted line) at projected radii $20 < R < 50$ kpc. The histogram shows the number of data sets out of 1000 which yielded a given percentage error in the mass within 50 kpc. (d) Histogram illustrating the reduced bias in mass estimates based on globular cluster data sets containing 100 objects at projected radii $20 < R < 50$ kpc for which proper motions have been obtained using *GAIA*.

data sets of 10 satellites each, drawn from a TF model density distribution with a DF of the form given in equation (8). The anisotropy scale r_a is taken as 166 kpc (which is the mean of the prior probability distribution over the allowed range of 2.5 to 1000 kpc). In carrying out this procedure, we use a Gaussian approximation to the actual DF, taking the velocity dispersions as the widths of the Gaussians. This approximation can very occasionally lead to the generation of satellites which are not bound – these are rejected from our data sets. Each data set is analysed using the algorithm described in Section 4, and the most likely value of the total mass of the halo is noted.

The solid histogram in Fig. 7(a) shows the number of data sets which yield a given percentage error in the mass estimate. There is a tendency to underestimate the mass, with ~50 per cent of estimates more than a factor of 2 smaller than the true value. Only ~14 per cent of estimates are within 20 per cent of the correct value. There is also a large spread in mass estimates – the average absolute deviation of the estimates about the mean is 49 per cent. It is reasonable to hope that the number of satellite galaxies could rise to perhaps 20 in the near future, given the successes of the ongoing surveys of the sky around Andromeda (Armandroff & Da Costa 1999; Karachentsev & Karachentseva 1999). The dotted histogram of Fig. 7(a) shows the effect of this increase – the systematic underestimate is still present, although it is somewhat less than that for the 10 satellite case. We conclude that there is a systematic tendency to underestimate the mass by a factor of 2 due solely to the size of the data set. This is coupled with a spread of order ~50 per cent.

As the number of data points becomes large, our prior probabilities become unimportant. With small data sets, our choice for priors can lead to systematic biases. WE99 suggested that this effect was significant for the Milky Way, as the customary priors tend to be biased towards radial anisotropy, while the data set, at least judging from the available proper motions, is not. For the case of the simulations reported in Fig. 7(a), the mean of the mass prior $1/M^2$ is less than the true mass, which partly accounts for the effect. However, this circumstance is only slightly improved if we switch to a mass prior of $1/M$, whose mean does correspond to the true mass. There is clearly scope for more work on the possible causes of bias of mass estimators with small data sets. Both underestimates and overestimates have been reported by others using virial mass estimators (e.g. Haller & Melia 1996; Aceves & Perea 1999). It seems likely that Bayesian estimators can also yield biased results of either sign, depending on the details of the potential, distribution function and priors. However, for our models, small data sets of radial velocities typically lead to underestimates.

6.2 Incompleteness

In order to study the effects of incompleteness, we generate data sets of 20 satellites in which the positions are chosen according to a TF profile with $a_s = 150$ kpc, while the velocities are chosen assuming a value of $a_s = 300$ kpc in the number density profile. When analysing the data, a value of $a_s = 150$ kpc is assumed. This is analogous to the observational situation in which the observed number density distribution may not correspond to the true distribution if the sample is incomplete. The measured velocities are, however, governed by the true velocity distribution.

Fig. 7(b) presents the results of performing 1000 such simulations. Comparing this histogram with the dotted histogram of Fig. 7(a), we see that the incompleteness has not degraded our ability to estimate the mass in any significant way. We therefore conclude that the (unknown) incompleteness of our satellite sample should not bias our mass estimate, provided that the incompleteness is unrelated to the kinematics of the satellites. However, one can imagine cases in which this could happen – for example, if there is a systematic tendency for the fainter satellites to move on different types of orbits than the brighter satellites. In this case, the magnitude limit enforces a kinematic bias which is difficult to model, but could have a deleterious effect on the resulting mass estimates. However, if the only incompleteness is due to magnitude limits in our surveys and is kinematically unbiased, then Fig. 7(b) shows us that the major worry is the small number of satellites and not the incompleteness of the sample.

6.3 Globular cluster data sets

We now examine the uncertainties in our mass estimates for the inner region of the M31 halo based on the globular clusters and planetary nebulae. Bearing in mind the ongoing searches (Perrett et al. 1999), our main motivation is to discover how many radial velocities are needed for reliable results. The solid histogram of Fig. 7(c) shows the results of estimates of the mass inside 50 kpc based on simulated data sets of 30 globular clusters with projected radii $20 \lesssim R \lesssim 50$ kpc drawn from a rotating DF of the form (14).

As in the case of the satellites, there is a systematic bias towards underestimates of the mass, although this is less pronounced than the factor of 2 bias observed in the satellite case. The spread in mass estimates is also reassuringly small (∼15 per cent). The dotted histogram in Fig. 7(c) shows the results of simulations of data sets consisting of 100 globular clusters at projected radii out to 50 kpc. This histogram demonstrates the value of searching for globular clusters orbiting M31 at larger radii. The systematic bias in the mass estimate is greatly reduced, and ∼90 per cent of the estimates lie within 10 per cent of the true value. The mass within 30 kpc can also be recovered to excellent accuracy (∼93 per cent of estimates lie within 10 per cent of the true answer).

7 CONCLUSIONS AND PROSPECTS

Our best estimate for the mass of the M31 halo based on the motions of satellite galaxies, planetary nebulae and globular clusters is $12.3 \times 10^{11}\,\mathrm{M}_{\odot}$. There is at least a factor of 2 uncertainty in this value due to the small sizes of the three tracer data sets. Using Monte Carlo simulations of data sets of 10 satellites, we have shown that there is a tendency to underestimate the mass with this algorithm when the data are very sparse – we find that 50 per cent of mass estimates underestimate the mass by more than a factor of 2. There is also a spread in mass estimates of order 50 per cent. Incorporating these into error bars on our mass estimate, we obtain $12.3^{+18}_{-6} \times 10^{11}\,\mathrm{M}_{\odot}$. For comparison, our earlier estimate for the Milky Way halo (WE99) was $19^{+36}_{-17} \times 10^{11}\,\mathrm{M}_{\odot}$. Although the error bars are large, we reach the surprising conclusion that *the total mass of M31 may well be less than that of the Milky Way.*

This is contrary to current opinion. Almost all recent authors have argued that M31 is the most massive member of the Local Group (e.g. Peebles 1989; Hodge 1992; Mateo 1998; Courteau & van den Bergh 1999). These authors adduce a number of pieces of evidence to support their viewpoint. The asymptotic value of the rotation curve of M31 seems to be ∼10 per cent higher than that of the Milky Way (Rubin & Ford 1970). The number of globular clusters in M31 is more than double that in the Milky Way (Fusi Pecci et al. 1993). The scalelength of the M31 disc exceeds that of the Milky Way (Walterbos & Kennicutt 1988). The face-on *B*-band absolute magnitude of M31 is $M_{\mathrm{B}} = -21.1 \pm 0.4$, whereas that of the Milky Way is $M_{\mathrm{B}} = -20.5 \pm 0.5$ (Hodge 1992). On the other hand, the infrared luminosity of the Milky Way is much higher than that of M31 (Walterbos & Schwering 1987). The mass in hydrogen gas in the Milky Way also exceeds that in M31 (Hodge 1992).

The difficulty in all this is judging whether any of these statements are properly comparing like with like. M31 has Hubble type Sb, whereas the Hubble type of the Milky Way is certainly later, perhaps Sbc or Sc (e.g. Gilmore, King & van der Kruit 1989). On such grounds alone, it is natural to expect that M31 has a larger bulge than the Milky Way. Late-type spirals are gas-rich, and so it is also natural to expect the mass in gas in the Milky Way to exceed that of M31. The relative number of globular clusters is a poor argument, as it is only weakly correlated with total mass (e.g. Ashman & Zepf 1998). There is also no correlation between the satellite velocity dispersion in the outer halo of a galaxy and the rotation velocity of its disc (Zaritsky et al. 1997). Thus a higher disc rotation velocity does not necessarily imply a more massive halo.

We believe that the mass within ∼30 kpc is greater for Andromeda than for the Milky Way, though probably only by about 20 per cent. The best guide to total mass is provided by the kinematics of distant tracers like the satellite galaxies. Our analysis of both galaxies is the most complete and sophisticated to date, and it suggests that the total mass of the M31 halo is probably less than that of the Milky Way. Beyond ∼30 kpc, the mass-to-light ratio of M31 seems to increase more slowly than in the Milky Way.

There is a pressing need for more data on objects in the halo of M31, if we are to consolidate this result. There are a number of lines of attack. First, there are five satellites of M31 whose radial velocities have not yet been measured, namely And I, And III, And V, Pegasus II (And VI) and Cassiopeia (And VII). The measurement of the radial velocities of these galaxies is being carried out at present (Grebel, private communication). This will increase by 50 per cent the number of tracer objects at large radii, and it will be interesting to see how the mass estimate changes. There is even cause for optimism that the data set will increase in size. The current rate of discovery of dwarf spheroidals of M31 (And V, And VI and And VII were discovered in 1998) emphasizes the number of satellites which have thus far been missed. Karachentsev & Karachentseva (1999) state that the north–south asymmetry in the distribution of satellites about M31 could imply that 3–5 satellites of M31 have escaped detection due to Galactic extinction and the extended cirrus fields in the vicinity of M31. A second line of attack is the discovery and exploitation of halo globular clusters and planetary nebulae (Bridges 1999; Perrett et al. 1999). Based on a comparison with the Milky Way globular cluster system, Fusi Pecci et al. (1993) estimate that outside 20 kpc there are likely to be ∼30 globular clusters brighter than $V = 18$. Identifying these distant bright clusters and measuring their radial velocities is an important target for constraining the total mass. The surveys in progress are concentrated in the central regions and contain only a few objects outside ∼20 kpc (Perrett, private communication). These are primarily useful for measuring the mass distribution in the inner parts – for example, a data set of 100 globular clusters with radial velocities would allow us to determine the mass within 30 kpc to within 10 per cent (see Fig. 7c). The number of planetary nebulae in M31 is known to be of the order of 10^4 (Nolthenius & Ford 1987). Many hundreds of planetary nebulae lie in the halo, and are invaluable as probes of the potential in regions where no other tracers have been found. Nowadays, these can be identified relatively easily with wide-field imaging using O III and continuum filters, and their velocities can be found with multi-object spectroscopy. So there are real prospects that much larger data sets will be available soon.

Within the decade, astrometric satellites will allow the determination of the proper motions of some of the globular clusters of M31. While this is beyond the reach of current ground-based instruments, the proposed *Global Astrometric Interferometer for Astrophysics* (*GAIA*) satellite will scan the whole sky and will perform astrometry on all objects brighter than $V = 20$.The apparent magnitudes of the unresolved cores of M31's bright globular clusters are typically around $V \approx 16$–17. Fig. 7(d) shows how the mass estimate within 50 kpc is affected by the addition of proper motion measurements for a data set of 100 globular clusters with $20 < R < 50$ kpc. The systematic bias visible in the solid histogram of Fig. 7(c) when only radial velocities are used is absent when proper motion data are available, and the spread in mass estimates is less than 10 per cent. The mass inside 30 kpc is also recovered with high confidence with the spread in mass estimates being ∼5 per cent.

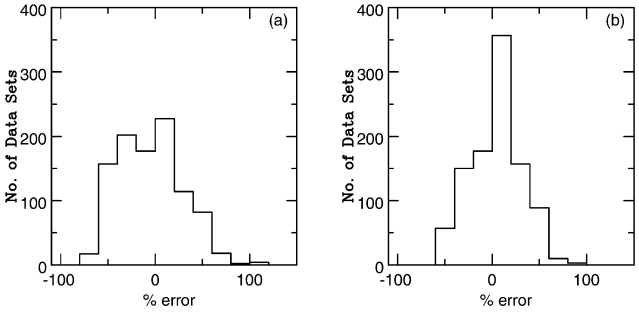

Figure 8. (a) Histogram showing the spread in mass estimates based on satellite data sets containing 10 objects at radii $20 < r < 500$ kpc whose proper motions have been measured using *SIM* and *GAIA*. The histogram shows the number of data sets out of 1000 which yielded a given percentage error in the total mass M. (b) As in (a), but for data sets of 20 satellites.

It will also be possible to obtain proper motions for some or all of the M31 dwarf galaxy satellites. In this case, the proposed *Space Interferometry Mission* (*SIM*) satellite is perhaps the most appropriate instrument to use. *SIM* is a pointing instrument. It will study fewer objects than *GAIA*, but with greater accuracy. *SIM* is planned to have an astrometric precision of $2\,\mu\mathrm{as\,yr}^{-1}$ for objects with $V = 20$. Almost all the Local Group members have at least some stars with magnitudes brighter than $V = 20$, making proper motion determinations feasible. The brighter objects, like M32 and M33, have $\sim 10^4$ stars with $V < 20$, while even the fainter ones, like IC 10 and NGC 147, have ~ 10. At the distance of M31, a proper motion uncertainty of $2\,\mu\mathrm{as\,yr}^{-1}$ corresponds to an error in the velocity transverse to the line of sight of $\sim 7\,\mathrm{km\,s}^{-1}$. Fig. 8(a) shows how the systematic underestimate is removed even if we only measure the proper motions of the 10 satellites which currently have radial velocities. The spread in mass estimates is still large (the average absolute deviation about the mean is ~ 27 per cent of the true mass estimate), as there are still only 10 data points. In the optimistic case in which the satellite data set swells to 20 and a combination of *SIM* and *GAIA* obtain all the proper motions, Fig. 8(b) shows that the mass estimates are much more strongly peaked around the true answer, and the spread is reduced to ~ 22 per cent of the true mass.

The masses of the Milky Way and the Andromeda galaxies are fundamental parameters that we need to know to understand the Local Group. Although our investigations have convinced us that the masses are rather imperfectly known at present, there are excellent prospects for improvement in the very near future.

ACKNOWLEDGMENTS

NWE thanks the Royal Society for financial support, while MIW acknowledges help from a Scatcherd Scholarship. We thank Tim de Zeeuw and Gerry Gilmore for information on the *GAIA* satellite, as well as James Binney and Scott Tremaine for useful advice. We are grateful to Terry Bridges, Dave Carter and Kathy Perrett for keeping us informed of their globular cluster and planetary nebulae surveys of M31. Kathy Perrett kindly fowarded data on the positions and radial velocities of the outermost globular clusters in advance of publication.

REFERENCES

Aceves H., Perea J., 1999, A&A, 345, 439
Armandroff T. E., Da Costa G. S., 1999, in Whitelock P., Cannon R., eds, Proc. IAU Symp. 192, The Stellar Content of Local Group Galaxies. Astron. Soc. Pac., San Francisco, p. 203
Arnaboldi M., Napolitano N., Capaccioli M., 2000, in Combes F., Mamon G., Charmandaris V., eds, ASP. Conf. Ser., Vol. 197, Galaxy Dynamics: From the Early Universe to the Present. Astron Soc. Pac., San Francisco, p. 103
Ashman K., Zepf S., 1998, Globular Cluster Systems. Cambridge Univ. Press, Cambridge
Bahcall J. N., Tremaine S. D., 1981, ApJ, 244, 805
Barmby P., Huchra J. P., Brodie J. P., Forbes D. A., Schroder L. L., Grillmair C. J., 2000, AJ, 119, 727
Binney J., Tremaine S., 1987, Galactic Dynamics. Princeton Univ. Press, Princeton
Braun R., 1991, ApJ, 372, 54
Bridges T., 1999, in Merritt D., Sellwood J. A., Valluri M., eds, ASP Conf. Ser., Vol. 182, Galaxy Dynamics – A Rutgers Symposium. Astron. Soc. Pac., San Francisco, p. 415
Côté P., Mateo M., Olszewski E. W., Cook K. H., 1999, ApJ, 526, 147
Courteau S., van den Bergh S., 1999, AJ, 118, 337
Crampton D., Cowley A., Schade D., Chayer P., 1985, ApJ, 288, 494
Crotts A. P. S., 1992, ApJ, 399, L43
Crotts A. P. S., Tomaney A., 1996, ApJ, 473, L87
Deharveng J. M., Pellet A., 1975, A&A, 38, 15
Djorgovski S., Meylan G., 1994, AJ, 108, 1292
Einasto J., Rümmul U., 1970, in Becker W., Contopoulos G., eds, Proc. IAU Symp. 38, The Spiral Structure of our Galaxy. Reidel, Dordrecht, p. 51
Elson R. A. W., Walterbos R. A. M., 1988, ApJ, 333, 594
Evans N. W., 1993, MNRAS, 260, 191
Evans N. W., Wilkinson M. I., 2000, in Menzies J. W., Sackett P. D., eds, ASP. Conf. Ser., Vol., Microlensing 2000: A New Era of Microlensing Astrophysics. Astron. Soc. Pac., San Francisco, in press
Evans N. W., Häfner R. M., de Zeeuw P. T., 1997, MNRAS, 286, 315
Feast M., 1999, in Whitelock P., Cannon R., eds, Proc. IAU Symp. 192, The Stellar Content of Local Group Galaxies. Astron. Soc. Pac., San Francisco, p. 203
Federici L., Bònoli F., Ciotti L., Fusi Pecci F., Marano B., Lipovetsky V. A., Neizvestny S. I., Spassova N., 1993, A&A, 274, 87
Ford H. C., Ciardullo R., Jacoby G. H., Hui X., 1989, in Torres-Peimbert S., ed., Proc. IAU Symp. 131, Planetary Nebulae. Kluwer, Dordrecht, p. 335
Fusi Pecci F., Cacciari L., Federici L., Pasquali A., 1993, in Smith G. H., Brodie J. P., eds, ASP. Conf. Ser. Vol. 48, The Globular Cluster–Galaxy Connection. Astron. Soc. Pac., San Francisco, p. 410
Gilmore G., King I. R., van der Kruit P. C., 1989, The Milky Way as a Galaxy. University Science Books, Mill Valley, California
Gottesman S. T., Davies R. D., 1970, MNRAS, 149, 263
Grebel E. K., 1999, in Whitelock P., Cannon R., eds, Proc. IAU Symp. 192, The Stellar Content of Local Group Galaxies. Astron. Soc. Pac., San Francisco, p. 17
Gunn J., 1975, Comments Astrophys. Space, 6, 7
Haller J. W., Melia F., 1996, ApJ, 464, 774
Hartwick F., Sargent W., 1974, ApJ, 190, 283
Heisler J., Tremaine S. D., Bahcall J. N., 1985, ApJ, 298, 8
Hénon M., 1973, A&A, 24, 229
Hodge P., 1975, BAAS, 1, 506
Hodge P., 1992, The Andromeda Galaxy. Kluwer Academic Press, Dordrecht
Huchra J. P., Stauffer J., van Speybroeck L., 1982, ApJ, 259, L57
Huchra J. P., Kent S. M., Brodie J. P., 1991, ApJ, 370, 495
Kahn F., Woltjer L., 1959, ApJ, 130, 705
Karachentsev I. D., Karachentseva V. E., 1999, A&A, 341, 355
Karachentsev I. D., Makarov D. I., 1996, AJ, 111, 794
Karachentsev I. D., Tikhonov N. A., Sazonova L. N., 1994, Astron. Letters, 20, 84
Kendall M., Stuart A., 1977, The Advanced Theory of Statistics. Griffin, London
Kent S. M., Huchra J. P., Stauffer J., 1989, AJ, 98, 2080

Kerins E. J., Carr B. J., Evans N. W., Hewett P., Lastennet E., Le Du Y., Melchior A.-L., Smartt S., Valls-Gabaud D., 2000, MNRAS, in press (astro-ph/0002256)
Kochanek C., 1996, ApJ, 457, 228
Kulessa A. S., Lynden-Bell D., 1992, MNRAS, 255, 105
Lee M. G., Freedman W. L., Madore B. F., 1993, in Nemec J. M., Matthews J. M., eds, New Perspectives on Stellar Pulsation and Pulsating Variable Stars. Cambridge Univ. Press, Cambridge, p. 92
Little B., Tremaine S. D., 1987, ApJ, 320, 493
Lynden-Bell D., 1999, in Whitelock P., Cannon R., eds, Proc. IAU Symp. 192, The Stellar Content of Local Group Galaxies. Astron. Soc. Pac., San Francisco, p. 39
Mateo M., 1998, ARA&A, 36, 435
Merritt D., 1985, AJ, 90, 1027
Nolthenius R., Ford H. C., 1987, ApJ, 317, 62
Osipkov L. P., 1979, Pis'ma Astr. Zh., 5, 77
Peebles P. J. E., 1989, ApJ, 344, L53
Perrett K., Hanes D., Bridges T., Irwin M., Carter D., Huchra J., Brodie J., Watson F., 1999, in Merritt D., Sellwood J. A., Valluri M., eds, ASP Conf. Ser. Vol. 182, Galaxy Dynamics – A Rutgers Symposium. Astron. Soc. Pac., San Francisco, p. 431
Roberts M., Whitehurst R., 1975, ApJ, 201, 327
Rood H. J., 1979, ApJ, 232, 699
Rubin V., Ford W., 1970, ApJ, 159, 379
Sargent W. L. W., Kowal C. T., Hartwick F. D. A., van den Bergh S., 1977, AJ, 82, 947
Schmoldt I., Saha P., 1998, AJ, 115, 2231
van den Bergh S., 1981, PASP, 93, 428
van den Bergh S., 1998, AJ, 116, 1688
van den Bergh S., 1999a, AJ, 117, 2211
van den Bergh S., 1999b, A&AR, 9, 273
van der Marel R. P., Magorrian J., Carlberg R. G., Yee H. K. C., Ellingson E., 2000, AJ, 119, 2038
Walterbos R. A. M., Kennicutt R. C., 1988, A&A, 198, 61
Walterbos R. A. M., Schwering P. B. W., 1987, A&A, 180, 27
Wilkinson M. I., 1999, PhD. thesis, Univ. Oxford
Wilkinson M. I., Evans N. W., 1999, MNRAS, 310, 645 (WE99)
Zaritsky D., Smith R., Frenk C. S., White S. D. M., 1997, ApJ, 478, 39

APPENDIX A: A REGULARIZING TRANSFORMATION

DFs of the form $l^{-2\beta}f(\varepsilon)$ present a difficulty when calculating the probabilities (24) or (26) since, for $\beta > 0$, they possess a singularity at $l = 0$. This singularity, however, is integrable for all $\beta < 1$. Van der Marel et al. (2000) refer to this problem, and use the substitution $s = \ln\tan\eta$ to remove the singularity. [We recall from Section 4.1 that (v_t, η) are polar coordinates in the plane of projection.] This substitution solves the problem for $0 < \beta < 1$, but only in the case of the projected probability distributions (26).

For the unprojected probability distributions (24), van der Marel et al.'s (2000) substitution regularizes the integral for $\beta < 1/2$. In order to calculate the probability (24) numerically for $1/2 < \beta < 1$, we have to make the additional transformation in velocity space $(v_t, \eta) \rightarrow (\lambda, \mu)$, where

$$\lambda = [v_t\cos(\theta_i + \alpha_i) + v_{r\odot,i}\sin(\theta_i + \alpha_i)]^{2-2\beta},$$
$$\mu = \arctan\left[\frac{\eta v_t}{v_t\cos(\theta_i + \alpha_i) + v_{r\odot,i}\sin(\theta_i + \alpha_i)}\right] \qquad \text{(A1)}$$

in the region of the singularity.

This paper has been typeset from a TEX/LATEX file prepared by the author.